Stability in the Reconfiguration of Cable-Driven Parallel Robot Using Multiple Mobile Cranes

Hor Tan, Rizal Muntashir, Latifah Nurahmi, Bambang Pramujati, Ari Kurniawan, Unggul Wasiwitono, Stéphane Caro

Stability in the Reconfiguration of Cable-Driven Parallel Robot Using Multiple Mobile Cranes

Abstract: This paper presents a stability analysis based on the Zero Moment Point (ZMP) concept during the reconfiguration of a Cable-Driven Parallel Robot (CDPR) using three mobile bases. Each mobile base can be driven forward and backward, and it has a crane that can be moved up and down, to which a cable connected to the end effector is attached. The ZMP should stay within the designated support boundaries to prevent the robot from tumbling. Therefore, the next positions of the cable exit point are changed by applying two reconfiguration schemes to the robot: (I) changing the mobile base position and (II) altering the crane length. Kinetostatic models of both reconfiguration schemes are formulated such that the wrench matrix can be computed to find the cable tension. A fifth-degree polynomial test trajectory is defined so as to be followed by the end-effector. When executing a prescribed trajectory, the sequence of the mobile base position and the crane length are optimized by continuously considering the robot stability based on ZMP. Without reconfiguration, the mobile cranes cannot handle high cable tension; thus, they tip over. By performing two reconfiguration schemes, the whole system can be constantly maintained in equilibrium, and the robot's workspace can be enlarged; therefore, the tipping over can eventually be avoided. An experimental setup is prepared to demonstrate and confirm the mathematical models of both reconfiguration scenarios.

1. Introduction

Many researchers are interested in Cable-Driven Parallel Robots (CDPR) due to their large workspace, heavy payload capacity, and high velocity. CDPR has been employed in several applications in the industrial field, and some prototypes have been fabricated, for example, IPAnema [1], and COGIRO [2, 3]. Inverse kinematics, static equilibrium, dynamics, stiffness, and the workspace of CDPR were investigated in [4, 5]. Interval analysis and cable interference were taken into account in [6] to synthesize the workspace of cable-driven leg training in a gait training machine. The workspace boundaries, leading to the definition of wrench-closure workspace, are numerically determined in [7] which allows the designers to decide whether a pose is acceptable. Wrench-Feasible-Workspace (WFW) is defined as the set of mobile platform poses where the cables can compensate any wrench; therefore, each cable tension remains within a designated tension range [8,9]. The methodology to trace the WFW based on Available-Wrench-Set (AWS) for mobile CDPR was proposed in [10, 11]. Two approaches, the convex hull and the hyperplane shifting methods, were introduced to determine the AWS. These approaches were tested for a suspended CDPR performing three-degree-of-freedom (3-DOF) motion to obtain a large workspace. The workspace of tendon-based Stewart platforms was analyzed in [12]. In [13], the distribution of cable tensions was shown for a number of trajectories of the end-effector, for example, horizontal or spherical trajectories. The cable tension remains positive and continuous at all times. The S-curve trajectory planning method, which was evaluated for polynomial and trigonometric models, was introduced and formulated in [14]. Two separate types of trajectories in joint space were evaluated i.e. lower and higher-order polynomials. The functions for a lower-order polynomial are parabolic and cubic. Septic and nonic were analyzed as higher-order polynomials [15].

In [16], a concept of reconfiguration was applied to CDPR by attaching idler pulleys to the moving platform to enhance manipulation capabilities and cable tension distribution. A similar approach was employed in [17] by installing cable-and-pulley differentials on the moving platform. It aims to anticipate the complicated pulley kinematics due to modeling inaccuracies. In [18], the pulleys can be positioned at a set of possible reconfigurations via optimization. A systematic approach to design an optimal reconfigurable CDPR was presented in [19]. Reconfigurable CDPR has been used for several applications, such as search-and-rescue operations [20], medical rehabilitation [21], airplane industries [22, 23], and building constructions [24–26].

In [27], the mobile bases were combined with CDPR due to its excellent mobility performance and payload capacity. Four mobile bases are linked to the moving platform by four cables, which enables the robot to perform 4-DOF motion [28]. In [29–31], four mobile bases were employed, each consisting of two cables. The eight cables are connected to the moving platform, which is equipped with a gripper. The robot can be easily reconfigured and adapted to the environment thanks to mobile bases. The passive and active mobile bases are able to adjust the geometry of the CDPR according to the environment. A planar mobile CDPR was developed in [32] using two

mobile bases, each composed of two cables.

The four-wheeled mobile robots are commonly used to support the CDPR since their symmetrical architecture poses better load-carrying capacity and good motion stability. According to [33], the robot's motion stability is the robot's ability to return to the balance state when influenced by the external forces/moments such that the robot performs a smooth motion. The methods for stability analysis mainly consist of static analysis [34, 35] and dynamic analysis [36]. The most common static and dynamic stability criterion is the Zero-Moment-Point (ZMP), which is widely applied by the legged-locomotion and wheeled-locomotion robot communities. ZMP defines the point on the ground where the sum of the horizontal components of moments caused by the gravity and inertia forces is zero. The robot is stable if the ZMP is located inside the support boundaries. The horizontal distance between the ZMP and the support boundaries represents the tendency of the robot to tip over; hence, the ZMP concept is most suitable for motion on the horizontal plane or planar motion. The tipping-over rate is generally determined in the form of the moment equilibrium equations in static rate. It is possible to define the tipping-over stability for the dynamic characteristics [37]. The quadruped robot developed in [38] can adjust the next feet' position based on the ZMP location to maintain stability when it bumps into unpredictable terrain. It proves that, in general, the robot's stability depends on the position of the next support that is able to supply the necessary moments to counter the tipping over.

Inspired by the above ideas, the CDPR in this paper is developed using three four-wheeled mobile bases equipped with a vertical crane. The cable exit points' next position can be altered so that the CDPR can maintain its stability despite the sudden spike in cable tension. The CDPR will stay stable if the ZMP is located within the ground-front wheel contact point and the ground-rear wheel contact point of the mobile base. To keep the ZMP always within the predefined boundaries, the next position of the cable exit points is modified in two ways: (I) driving the mobile base back and forth and (II) moving the crane up and down. The kinetostatic models of both techniques are formulated and included in the ZMP computation, which becomes the paper's major contribution. A set of positions of the cable exit point are determined via optimization; hence, they can provide the required moments to prevent the robot from tipping, and a prescribed trajectory can be smoothly executed. An experimental setup to confirm the reconfiguration models is prepared and the results corroborate the developed hypotheses. To the best of the authors' knowledge, although a number of researches have been dedicated to reconfigurable CDPR, considering the ZMP in reconfigurable CDPR by using the mobile base and crane to maintain stability has not been discussed.

This paper is organized as follows: Section 2 describes the robot description and its reconfiguration scenarios. Section 3 derives the kinetostatic model of the system. Section 4 discusses the ZMP to evaluate the mobile base's and crane's stability when the end-effector follows a trajectory. Section 5 deals with the optimization to find the position of mobile bases and crane lengths during reconfiguration. Section 6 presents the prototype development and experiment, and the results are presented and discussed in Section 7. Finally, the conclusions are summarized in Section 8.

2. Robot Description and Reconfiguration Schemes

The schematic and parameterization of a CDPR with three mobile cranes are shown in Fig. 1. The robot consists of three mobile cranes of local coordinate $\mathscr{L}(O_i, u_i, v_i, w_i)$, where $i = 1,2,3$. Each mobile crane is located at the local origin O_i with distance ρ_i from the global origin O of global coordinate $\mathscr{F}(O,X,Y,Z)$, and the angle γ_i is measured counterclockwise from X-axis as depicted in Fig. 1(b).

The detailed vector diagram of each cable and the mobile base is illustrated in Fig. 2. The cables are linked from exit point A_i to point mass P. Exit point A_i is located at the pulley's center and connected to the crane at point A_i'. Point B_i is the connecting point from the mobile base to the crane.

Position vectors of exit point A_i in fixed coordinate ($\mathscr{F}$) are expressed by $\mathbf{a}_i^{\mathscr{F}}$, and it consists of the mobile base position $\rho_i^{\mathscr{F}}$ and crane length vectors $\mathbf{r}_i^{\mathscr{F}}$. Overall, vector $\mathbf{a}_i^{\mathscr{F}} = [a_{xi}, a_{yi}, a_{zi}]^T$ can be defined as follows:

$$\begin{aligned} \mathbf{a}_i^{\mathscr{F}} &= \rho_i^{\mathscr{F}} + \mathbf{r}_i^{\mathscr{F}} \\ &= \hat{\mathbf{v}}_i^{\mathscr{F}} \rho_i + \hat{\mathbf{w}}_i^{\mathscr{F}} r_i \end{aligned} \tag{1}$$

where ρ_i and r_i are, respectively, the mobile base position and the crane length. The unit vectors $\hat{\mathbf{v}}_i^{\mathscr{F}}$ and $\hat{\mathbf{w}}_i^{\mathscr{F}}$ express the direction of the mobile base and the crane, such that:

$$\hat{\mathbf{v}}_i^{\mathscr{F}} = \begin{bmatrix} \cos\gamma_i \\ \sin\gamma_i \\ 0 \end{bmatrix} \qquad \hat{\mathbf{w}}_i^{\mathscr{F}} = \begin{bmatrix} 0 \\ 0 \\ 1 \end{bmatrix} \tag{2}$$

where the orientation of all three mobile bases are respectively defined by: $\gamma_1 = 90^\circ$, $\gamma_2 = 210^\circ$, and $\gamma_3 = 330^\circ$.

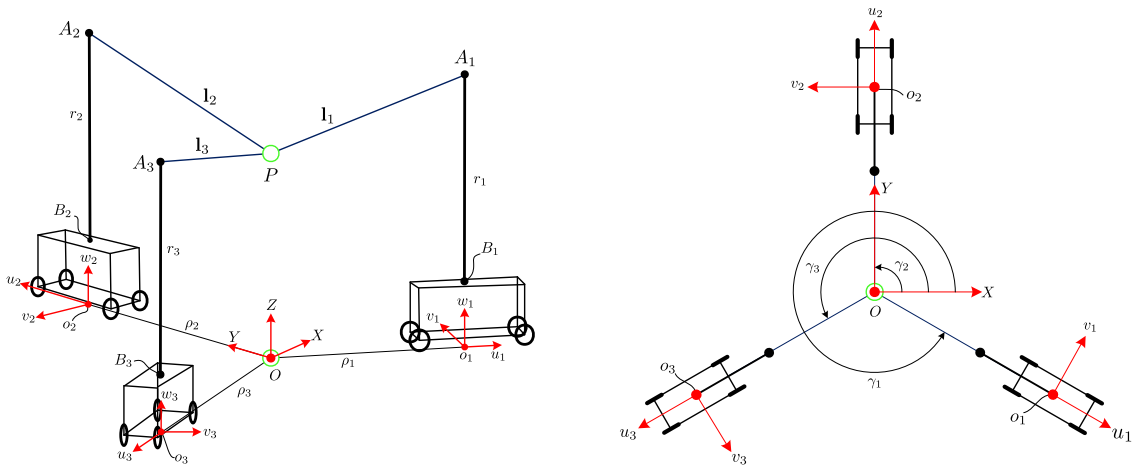

(a) Isometric view

(b) Top view

Fig. 1: Robot Description

The end-effector is considered to be a point mass P, of coordinate vector $\mathbf{p} = [p_x, p_y, p_z]^T$. Therefore, the loop-closure equation corresponding to each cable can be defined as follows:

$$\mathbf{l}_i^{\mathscr{F}} = \rho_i^{\mathscr{F}} + \mathbf{r}_i^{\mathscr{F}} - \mathbf{p} \tag{3}$$

The relationship between a point mass and exit point can be defined as the cable length l_i, as:

$$l_i = \left\| \mathbf{l}_i^{\mathscr{F}} \right\| = \sqrt{(\rho_i^{\mathscr{F}} + \mathbf{r}_i^{\mathscr{F}} - \mathbf{p})^T (\rho_i^{\mathscr{F}} + \mathbf{r}_i^{\mathscr{F}} - \mathbf{p})} \tag{4}$$

Accordingly, the unit vector of each cable $\hat{\mathbf{u}}_i^{\mathscr{F}}$ is computed as follows:

$$\hat{\mathbf{u}}_i^{\mathscr{F}} = \frac{\mathbf{l}_i^{\mathscr{F}}}{\left\| \mathbf{l}_i^{\mathscr{F}} \right\|} \tag{5}$$

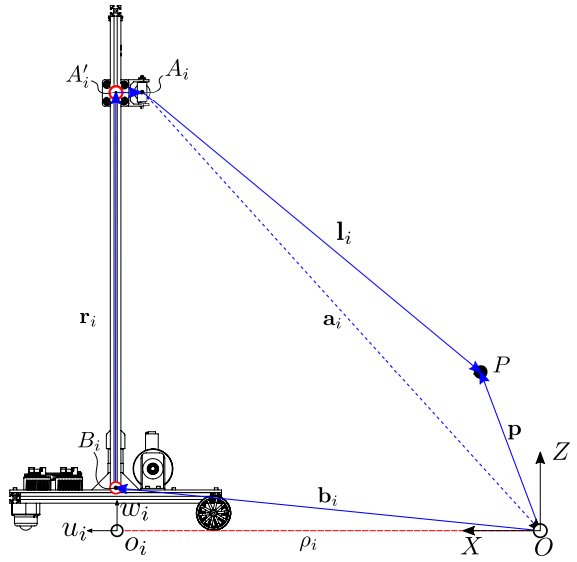

Fig. 2: Geometric description of a mobile base

In this paper, the concept of reconfiguration is introduced to be applicable to the developed CDPR; hence, its workspace can be enlarged and tipping can be avoided when tracking a given trajectory. Two reconfiguration scenarios are defined by moving the crane up and down and by driving the mobile base forward and backward, as follows:

1. **Reconfiguration I: mobile base reconfiguration**
   The three mobile bases are driven forward and backward such that their position reaches a minimum and maximum distances, i.e. $\rho_{i_{min}} = 1m$ and $\rho_{i_{max}} = 1.5m$, as shown in Fig. 3(a) by blue arrows).

2. **Reconfiguration II: crane reconfiguration**
   The crane is retracted and extended up to its minimum and maximum lengths, respectively, i.e. $r_{i_{min}} = 0.53m$ and $r_{i_{max}} = 0.83m$, as shown in Fig. 3(b) by blue arrows.

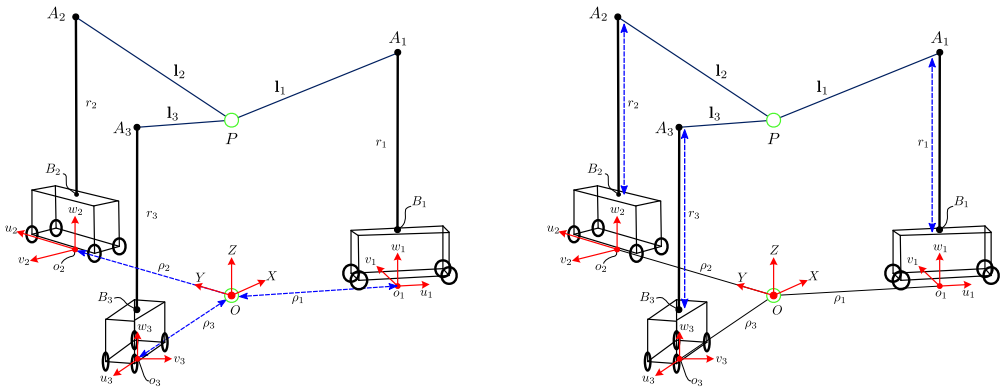

(a) Reconfiguration I (mobile base)

(b) Reconfiguration II (crane)

Fig. 3: Reconfiguration Schemes

3. Kinetostatic Model

3.1. End-effector

The paper context is the robot should move at relatively low velocities and accelerations, and be stable within a large workspace. The cables are assumed to be non-elastic and mass-less. As a consequence, the dynamics effects to the system are omitted and the computations in this paper follow a quasi-static fashion. The equation of static equilibrium at point P is expressed as follows:

$$\mathbf{W}\tau + \mathbf{w}_e = \mathbf{0} \tag{6}$$

where $\tau = [\tau_1, \tau_2, \tau_3]^T$ is the cable tensions vector, and $\mathbf{w}_e = [0, 0, -mg]^T$ is the gravitational force acting at point mass P. The gravity vector is denoted by $\mathbf{g} = [0, 0, -g]^T$ where $g = 9.8m.s^{-1}$. Since the wrench matrix $\mathbf{W}$ is a square matrix, then the cable tensions can be computed as follows:

$$\tau = -\mathbf{W}^{-1}\mathbf{w}_e \tag{7}$$

and the cable force $\mathbf{f}_i$ can be expressed as follows:

$$\mathbf{f}_i = \hat{\mathbf{u}}_i^{\mathscr{F}} \tau_i \tag{8}$$

The wrench matrix $\mathbf{W}$ of reconfiguration scenarios I and II are computed from the transpose of the Jacobian matrices, respectively, as:

$$\mathbf{W} = \begin{cases} \mathbf{J}_{\mathrm{I}}^T, & \text{for reconfiguration scheme I,} \\ \mathbf{J}_{\mathrm{II}}^T, & \text{for reconfiguration scheme II.} \end{cases} \tag{9}$$

In the concept of reconfiguration applied to the developed robot, the mobile bases, and the cranes are allowed to move when the cables are in operation. Hence, the mobile bases and the cranes will travel with velocities $\dot{\rho} = [\dot{\rho}_1, \dot{\rho}_2, \dot{\rho}_3]^T$ and $\dot{\mathbf{r}} = [\dot{r}_1, \dot{r}_2, \dot{r}_3]^T$, respectively. If the cable velocity is $\dot{\mathbf{l}} = \left[\dot{l}_1, \dot{l}_2, \dot{l}_3\right]^T$, Eq. (3) can be derived with respect to time to obtain the following relationship:

$$\mathbf{A}\dot{\mathbf{l}} = \mathbf{B}\dot{\rho} + \mathbf{C}\dot{\mathbf{r}} - \dot{\mathbf{p}} \tag{10}$$

where matrices $\mathbf{A}$, $\mathbf{B}$, and $\mathbf{C}$ are respectively defined as follows:

$$\mathbf{A} = \begin{bmatrix} \hat{\mathbf{u}}_1^{\mathscr{F}} & \hat{\mathbf{u}}_2^{\mathscr{F}} & \hat{\mathbf{u}}_3^{\mathscr{F}} \end{bmatrix} \tag{11a}$$

$$\mathbf{B} = \begin{bmatrix} \hat{\mathbf{v}}_1^{\mathscr{F}} & \hat{\mathbf{v}}_2^{\mathscr{F}} & \hat{\mathbf{v}}_3^{\mathscr{F}} \end{bmatrix} \tag{11b}$$

$$\mathbf{C} = \begin{bmatrix} \hat{\mathbf{w}}_1^{\mathscr{F}} & \hat{\mathbf{w}}_2^{\mathscr{F}} & \hat{\mathbf{w}}_3^{\mathscr{F}} \end{bmatrix} \tag{11c}$$

Equation (10) should be treated separately for each reconfiguration scenario to determine the Jacobian matrices $\mathbf{J}_{\mathrm{I}}$ and $\mathbf{J}_{\mathrm{II}}$, as follows:

1. **Kinetostatic of reconfiguration I**
   In this reconfiguration scenario, the three mobile bases can adjust their position while the cranes are maintained to be constant, therefore Eq. (10) becomes:

$$\mathbf{A}\dot{\mathbf{l}} = \mathbf{B}\dot{\rho} - \dot{\mathbf{p}} \tag{12}$$

   To discard the velocity term $\mathbf{B}\dot{\rho}$ in Eq. (12), a diagonal and invertible matrix $\mathbf{E}$ is introduced. Matrix $\mathbf{E}$ is composed of the mobile base velocities as follows:

$$\mathbf{E} = \begin{bmatrix} \frac{\dot{\rho}_3}{\dot{\rho}_1} & 0 & 0 \\ 0 & \frac{\dot{\rho}_3}{\dot{\rho}_2} & 0 \\ 0 & 0 & 1 \end{bmatrix} \tag{13}$$

   By multiplying Eq. (12) with diagonal matrix $\mathbf{E}$, the velocity vector of the mobile base $\dot{\rho}$ is eliminated and the cable velocity can be computed, such that:

$$\begin{aligned} \mathbf{AE}\dot{\mathbf{l}} &= -\mathbf{E}\,\dot{\mathbf{p}} \\ \dot{\mathbf{l}} &= -\mathbf{E}^{-1}\mathbf{A}^{-1}\mathbf{E}\,\dot{\mathbf{p}} \\ \dot{\mathbf{l}} &= -\mathbf{J}_{\mathrm{I}}\,\dot{\mathbf{p}} \end{aligned} \tag{14}$$

   where $\mathbf{J}_{\mathrm{I}}$ is the Jacobian matrix of reconfiguration scenario I that maps the end-effector velocity into the cable velocities by considering the mobile base velocities.

2. **Kinetostatic of reconfiguration II**
   The crane lengths can be moved up and down and simultaneously keep the mobile base position constant. As a consequence, Eq. (10) can be written as follows:

$$\mathbf{A}\dot{\mathbf{l}} = \mathbf{C}\dot{\mathbf{r}} - \dot{\mathbf{p}} \tag{15}$$

   A matrix $\mathbf{F}$ is introduced to remove the velocity term $\mathbf{C}\dot{\mathbf{r}}$ in Eq. (15). Matrix $\mathbf{F}$ is a diagonal and invertible matrix that consists of the crane velocities as follows:

$$\mathbf{F} = \begin{bmatrix} \dot{r_2}\dot{r_3} & 0 & 0 \\ 0 & \dot{r_1}\dot{r_3} & 0 \\ 0 & 0 & -2\dot{r_1}\dot{r_2} \end{bmatrix} \tag{16}$$

   and Eq. (15) can be expressed as:

$$\begin{aligned} \mathbf{AF}\dot{\mathbf{l}} &= -\mathbf{F}\,\dot{\mathbf{p}} \\ \dot{\mathbf{l}} &= -\mathbf{F}^{-1}\mathbf{A}^{-1}\mathbf{F}\,\dot{\mathbf{p}} \\ \dot{\mathbf{l}} &= -\mathbf{J}_{\mathrm{II}}\,\dot{\mathbf{p}} \end{aligned} \tag{17}$$

   Matrix $\mathbf{J}_{\mathrm{II}}$ maps the end-effector velocity into the cable velocities by taking into account the crane velocities.

3.2. Mobile base

Three mobile cranes should satisfy the static equilibrium condition during the end-effector movement. The free-body diagram of the $i-th$ mobile crane is illustrated in Fig. 4. The mobile crane is said to be tipping if it turns over about the axis v_i, then the frontal and rear reaction forces can be written respectively, as follows:

$$\begin{aligned} \mathbf{f}_{fri} &= \mathbf{f}_{r1i} + \mathbf{f}_{r4i} \\ \mathbf{f}_{rri} &= \mathbf{f}_{r2i} + \mathbf{f}_{r3i} \end{aligned} \tag{18}$$

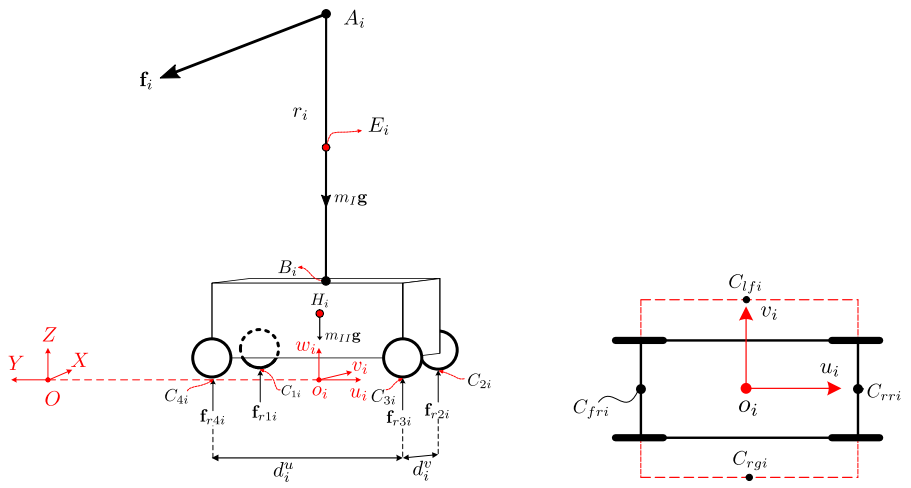

(a) Isometric view (b) Top view

Fig. 4: Free Body Diagram of Mobile Base

Based on Newton's law of motion, the force and moment equilibrium at point O is defined as follows:

$$\begin{gathered}\sum \mathbf{f} = 0 \\ \mathbf{f}_{fri} + \mathbf{f}_{rri} + m_I.\mathbf{g} + m_{II}.\mathbf{g} + \mathbf{f}_i = 0\end{gathered} \tag{19}$$

$$\begin{gathered}\sum \mathbf{M}_O = 0 \\ \mathbf{c}_{fri} \times \mathbf{f}_{fri} + \mathbf{c}_{rri} \times \mathbf{f}_{rri} + \mathbf{a}_i^{\mathscr{F}} \times \mathbf{f}_i + m_I.\mathbf{e}_i^{\mathscr{F}} \times \mathbf{g} \\ + m_{II}.\mathbf{h}_i^{\mathscr{F}} \times \mathbf{g} = 0\end{gathered} \tag{20}$$

where m_I and m_{II} are masses of the crane and mobile base, respectively. Their gravitational forces act at points E and H. $\mathbf{h}_i^{\mathscr{F}}$ and $\mathbf{e}_i^{\mathscr{F}}$ are the position vectors of the center of gravity H for the mobile base and E for the crane. $\mathbf{c}_{fri}$ and $\mathbf{c}_{rri}$ are the position vectors from the origin O to the frontal and rear sides of the mobile crane. $\mathbf{c}_{fri}$ and $\mathbf{c}_{rri}$ are defined as follows:

$$\begin{aligned}\mathbf{c}_{fri} &= \begin{bmatrix}\cos(\gamma_i)(\rho_i - L/2) \\ \sin(\gamma_i)(\rho_i - L/2) \\ 0\end{bmatrix} \\ \mathbf{c}_{rri} &= \begin{bmatrix}\cos(\gamma_i)(\rho_i + L/2) \\ \sin(\gamma_i)(\rho_i + L/2) \\ 0\end{bmatrix}\end{aligned} \tag{21}$$

The vertical components of frontal and rear reactions forces become:

$$f_{rri}^z = m_I g + m_{II} g - f_i^z - f_{fri}^z \tag{22}$$

$$\begin{gathered}f_{fri}^z = \big((e_i^y - c_{rri}^y)m_I g + (h_i^y - c_{rri}^y)m_{II} g + \\ (c_{rri}^y - a_i^y)f_i^z + a_i^z f_i^y\big) / \big(c_{fri}^y - c_{rri}^y\big)\end{gathered} \tag{23}$$

Equations (22) and (23) illustrate the effect of external forces acting on the cables on the stability of mobile cranes, which is defined by the value of reaction forces. It turns out that as the end-effector moves about a given path, the external forces may pull the cables, which eventually cause the mobile cranes to undergo tipping.

4. Stability based on ZMP

When the mobile bases move and execute a given task, the reaction forces are exerted between the wheels and the ground at the contact point. These reaction forces will be null if the robot tips over. Therefore, the tipping moment acting on the contact point is considered the moment's component [39].

In this paper, Zero Moment Point (ZMP) is used to evaluate the robot's stability, which can be defined as a point within the mobile bases where the sum of moments due to frontal and rear reaction forces is null. ZMP is expressed in the local coordinate $\mathscr{L}(u_i, v_i, w_i)$. Then, the cable force expressed in the local coordinate is as follows:

$$\mathbf{f}_i^{\mathscr{L}} = \begin{bmatrix} f_i^u \\ f_i^v \\ f_i^w \end{bmatrix} = \begin{bmatrix} f_i^x \cos(\gamma_i) + f_i^y \sin(\gamma_i) \\ -f_i^x \sin(\gamma_i) + f_i^y \cos(\gamma_i) \\ f_i^z \end{bmatrix} \tag{24}$$

At this instant, ZMP is applied to ensure the mobile crane is in static equilibrium while the end-effector moves along a prescribed path. As a result, the sum of moments at point o_i can be formulated for tipping analysis as follows:

$$\mathbf{M}_{o_i} - (\mathbf{f}_{fri} + \mathbf{f}_{rri}) \times \mathbf{d}_i = 0 \tag{25}$$

Where $\mathbf{d}_i$ is the vector position from the origin o_i to the edge of the mobile crane. The mobile crane will tip over about axis v_i, which means that ZMP will be within the points C_{1i} and C_{2i} or within the length d_i^u as shown in Fig. 4(b). From Equation (25), d_i^u is defined as follows:

$$d_i^u = \frac{a_i^u f_i^w - a_i^w f_i^u - m_I e_i^u g}{f_{fri}^w + f_{rri}^w} \tag{26}$$

Static-Feasible-Workspace [40] is characterized as the set of end-effector poses at a constant orientation for which the cables can maintain the static equilibrium under external force. The wrench is maintained to be positive in Static-Feasible-Workspace since the cable can be counteracted by the force applied onto the end-effector. In this section, the Static-Feasible-Workspace of the robot is computed when the robot is in non-reconfiguration state by solving Eq. (7), as shown in Fig. 5(a). To ensure that the end-effector is able to perform a task while the mobile cranes are in static equilibrium, point P must work inside the Static-Feasible-Workspace. The Static-Tipping-Free-Workspace can be generated by including the ZMP condition in the robot operation, i.e. by taking into account Eq. (23) into Eq. (7), as shown in Fig. 5(b). The size of the Static-Tipping-Free-Workspace is smaller, limiting the robot's movement. To deal with this issue, the reconfiguration schemes are introduced in Section 2, which can simultaneously enlarge the working coverage and manage the robot stability.

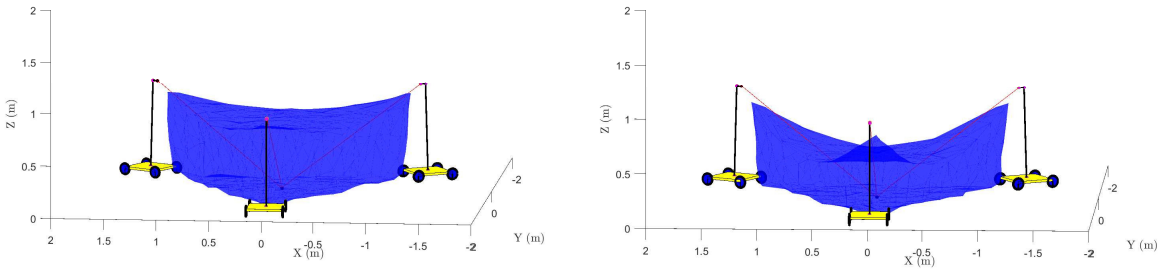

(a) Satis Feasible Workspace

(b) Static Tipping-Free Workspace

Fig. 5: Workspace

5. Reconfiguration Optimization

A trajectory, as shown in Fig. 6, is generated to assess the performance of the developed prototype, which will be demonstrated in Section 6. The prescribed trajectory is a succession of three segments from the first segment at $P_0 - P_1$ for $t = 0 - 5s$, the second segment at $P_1 - P_2$ for $t = 5 - 15s$, and the third segment at $P_2 - P_3$ for $t = 15 - 25s$. A fifth-order polynomial is used to obtain smooth velocity and acceleration profiles for each segment of the trajectory. Both reconfiguration schemes I and II will execute this trajectory. The trajectory is discretized into 300 equidistant points P. At each point, a set of positions of three mobile bases and a set of the length of three cranes (denoted by ρ_i and r_i, respectively) should be determined via optimization. The vectors consisting of the decision variables of reconfiguration schemes I and II are written as follows:

$$\mathbf{x} = \begin{cases} [\rho_1, \rho_2, \rho_3], & \text{for reconfiguration scheme I,} \\ [r_1, r_2, r_3], & \text{for reconfiguration scheme II.} \end{cases} \tag{27}$$

The boundaries of decision variables are based on the developed prototype, given as follows:

$$\begin{aligned} 1m \leq \rho_1, \rho_2, \rho_3 \leq 1.5m \\ 0.53m \leq r_1, r_2, r_3 \leq 0.83m \end{aligned} \tag{28}$$

Cable tensions have a big influence on the robot's static equilibrium. Likewise, cable velocities have a significant impact on the robot's motion. The optimization problem aims to simultaneously minimize the cable tensions and cable velocities to improve the robot's stability and motion smoothness. The motor mounted to the winch coils the cable with maximum cable velocity up to $0.015m/s$. Based on this technical requirement, the cable velocity

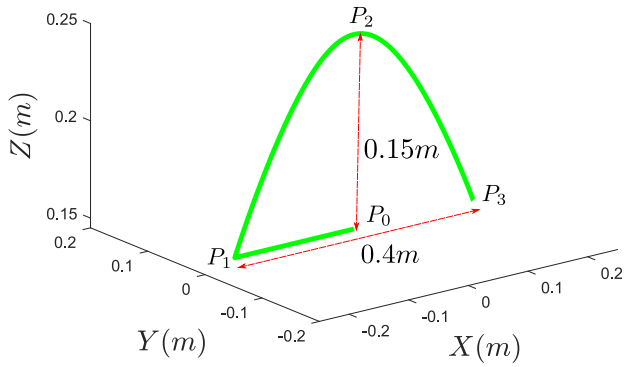

Fig. 6: Testing trajectory

becomes more important to reduce the motor burden. Therefore, the weighting factor $\lambda = 0.75$ is introduced in the formulation of the objective function as follows:

$$\mathscr{U}(\mathbf{x}) = (1-\lambda)\|\tau(\mathbf{x})\| + \lambda\|\dot{l}(\mathbf{x})\| \tag{29}$$

The use of a mobile base as a frame of CDPR, exposes a great risk of instability, which leads the robot to tumble. The robot stability becomes an important element during the optimization process at each point P of the trajectory. To satisfy this condition, the ZMP should always stay within the allowable distance d_i^u, representing the distance between the ground-front wheel contact point c_{fri}^u and the ground-rear wheel contact point c_{rri}^u. Eventually, the design problem can be formulated as follows:

$$\begin{aligned} \text{Find}: \ & \mathbf{x} \\ \text{Minimize}: \ & \mathscr{U}(\mathbf{x}) \\ \text{Subject to}: \ & c_{fri}^u \leq d_i^u \leq c_{rri}^u \end{aligned} \tag{30}$$

The optimum results along the prescribed trajectory are presented in Fig. 7. During reconfiguration scheme I, the mobile bases will change their positions following the optimal results shown in Fig. 7(a). Only the first and third mobile bases move. During reconfiguration scheme II, the cranes move up and down based on the optimal data given in Fig. 7(b). These designs will accordingly change the cable exit points that can prevent the robot from tipping and generate lower cable tensions. The experimentation of these designs is presented in Section 6

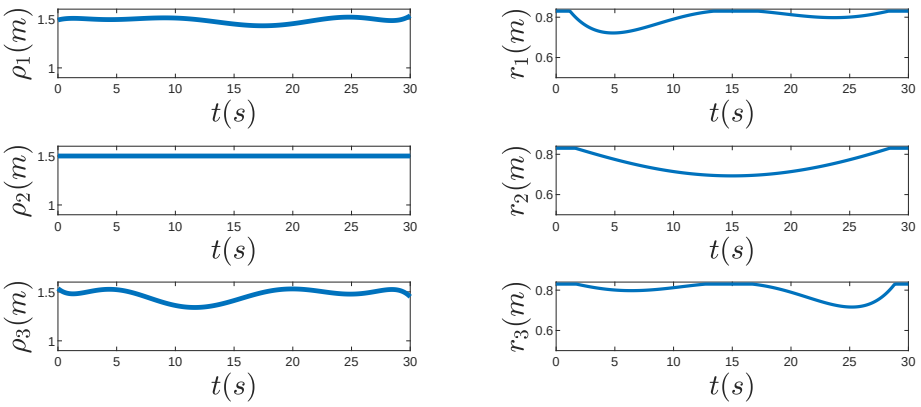

(a) Reconfiguration I

(b) Reconfiguration II

Fig. 7: Optimization Results

6. Prototype and Experiment

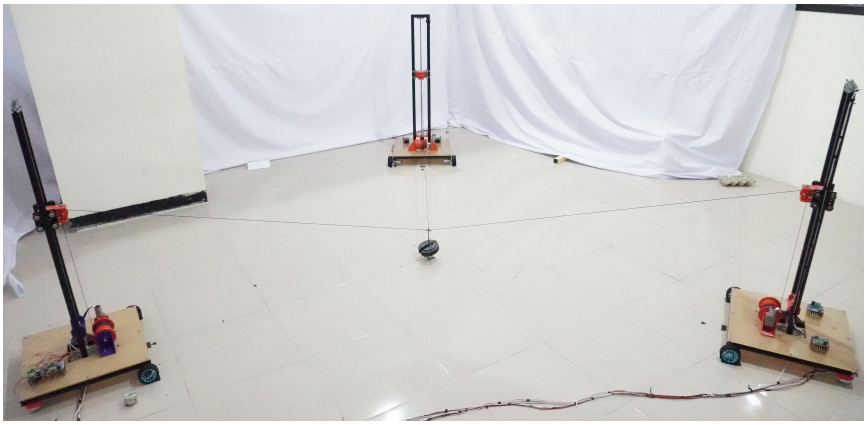

(a) Isometric view

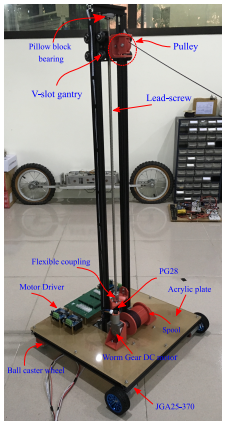

(b) Transmission

Fig. 8: Developed Prototype

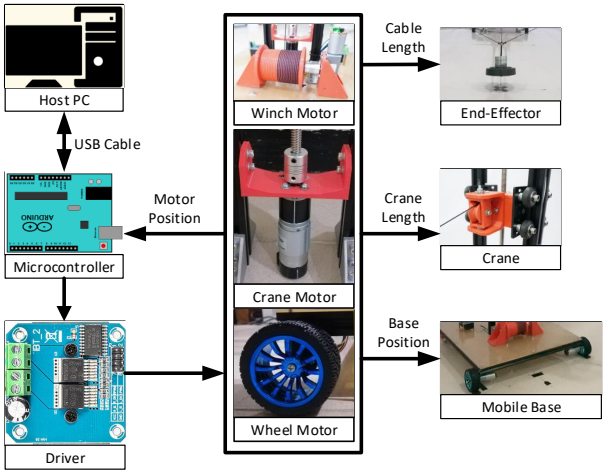

Fig. 9: Control architecture

The prototype of a cable-driven parallel robot with multiple mobile bases has been manufactured as shown in Fig. 8(a), and the transmission system of a mobile base is presented in Fig. 8(b). Each mobile base carries four actuators; namely: two actuators are used to drive the frontal wheels to move the mobile base, one actuator is used to actuate the lead screw to provide the crane motion at which the pulley is attached, and another one is to rotate the custom-made winch to coil the cables. The control system of the prototype is presented in Fig. 9, which is composed of a PC (equipped with ©MATLAB), a microcontroller, a motor driver, a transmission assembly divided into a winch motor with gearbox, a crane motor with lead screw, and the wheel motors.

7. Results and Discussion

Initially, the robot was tested to trace along the generated trajectory without adjusting the crane and mobile base. The computation of the tension distribution is shown in Fig. 10. The third cable tension jumps to $\tau_3 = 16.5N$, making the mobile base unstable and terminating the task around $t = 9s$. The third mobile base cannot handle high cable tension and finally collapses since the ZMP is not within the support boundaries. This robot's instability is corroborated by the experiment demonstrated in this video[1]. Figures 11(a)-(c) depicts the experimental results between the desired and measured cable lengths when the robot works without changing its cable exit points.

[1] Experiment of Non-reconfiguration

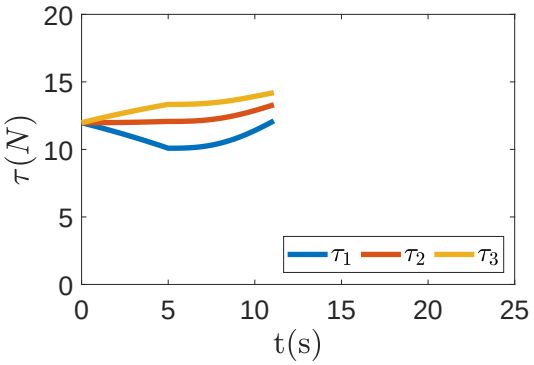

Fig. 10: Computational results of tension distribution without reconfiguration (tipping)

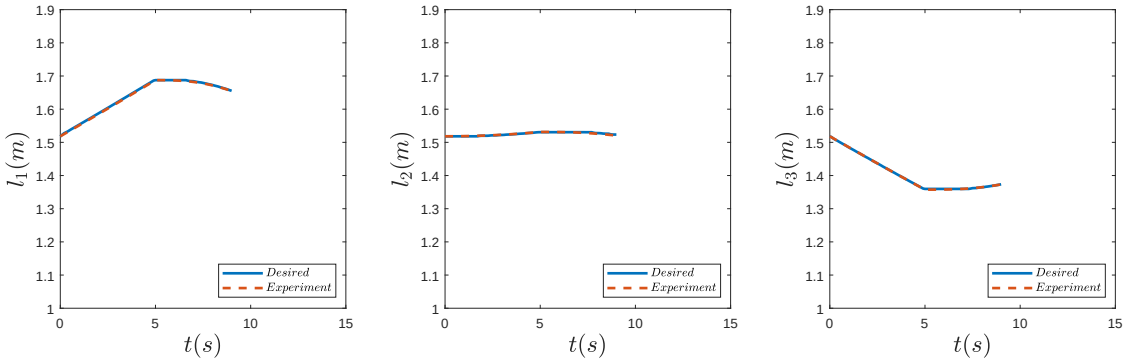

Fig. 11: Experimental results without reconfiguration

Then, two reconfiguration schemes were tested empirically as the end-effector executed the same trajectory. The tensions of the three cables are computed for reconfiguration I and II, and their distribution are respectively presented in Figs. 12(a) and 12(b). Optimizing the mobile base position and the crane length lowers cable tensions than the non-reconfiguration system. None of the mobile base turnover since the ZMP always stays within the support boundaries denoted by d_i^u, which justifies that the robot is able to maintain its stability during the task. The demonstration videos are provided to show the reconfiguration I and II[2]. Figures 13 and 14 depict the differences between the desired and measured cable lengths of reconfiguration I and II, respectively. The root mean square errors between the desired and obtained cable lengths during the reconfiguration I and II experiments are presented in Fig. 15. Despite the fact that errors exist, it shows that the completed experiments confirm the kinetostatic models derived for both reconfiguration schemes in Eqs. (14) and (17). The errors of cable lengths in reconfiguration I are higher than the ones in reconfiguration II, since driving the mobile bases that act as a frame for the whole robot will induce external moments to the end-effector that will eventually reduce the robot's rigidity. The slippage between the wheel and the ground might also contribute to it.

Cable tensions of reconfiguration II are lower than those of reconfiguration I. Likewise, the root mean square errors of cable length of reconfiguration II (less than 0.02) are significantly lower than those of reconfiguration I. According to these results, altering the crane will be more beneficial than changing the mobile base position, which means that reconfiguration II is more efficient for technical use.

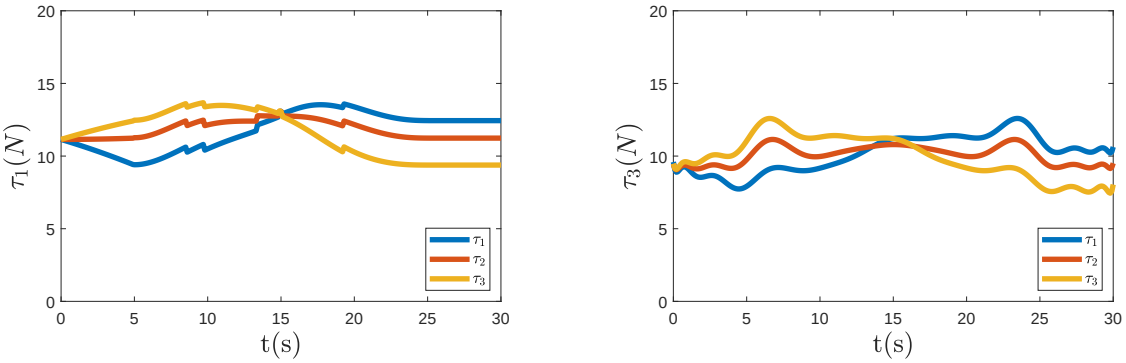

(a) Reconfiguration I (b) Reconfiguration II

Fig. 12: Computational results of tension distribution with reconfiguration

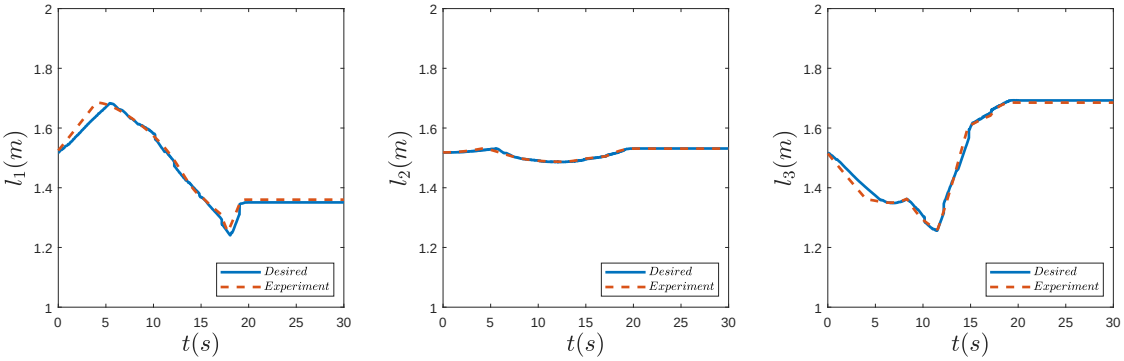

Fig. 13: Results from the experiments of reconfiguration case I

8. Conclusions

In this paper, the stability of a CDPR using three mobile cranes was investigated based on the concept of ZMP. The robot will remain stable if ZMP always stays within the specified support boundaries. Thus, the next positions of the cable exit point were shifted by implementing two reconfiguration schemes for the robot: (I) driving the mobile

[2]Experiment of Reconfiguration

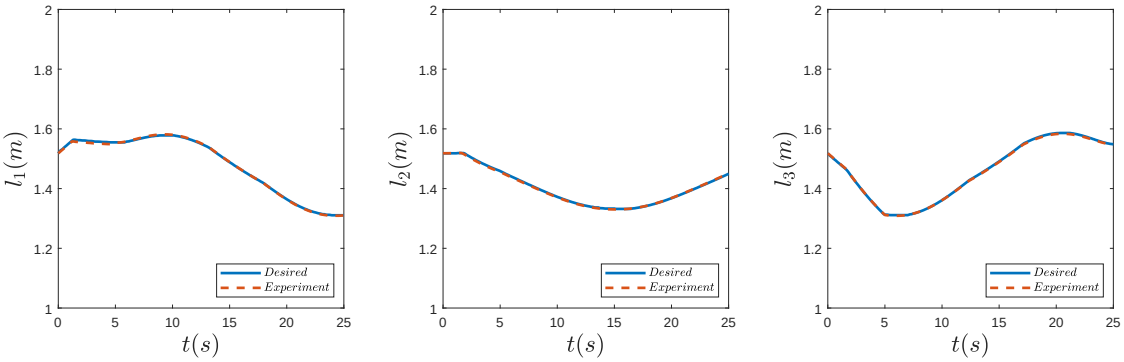

Fig. 14: Results from the experiments of reconfiguration case II

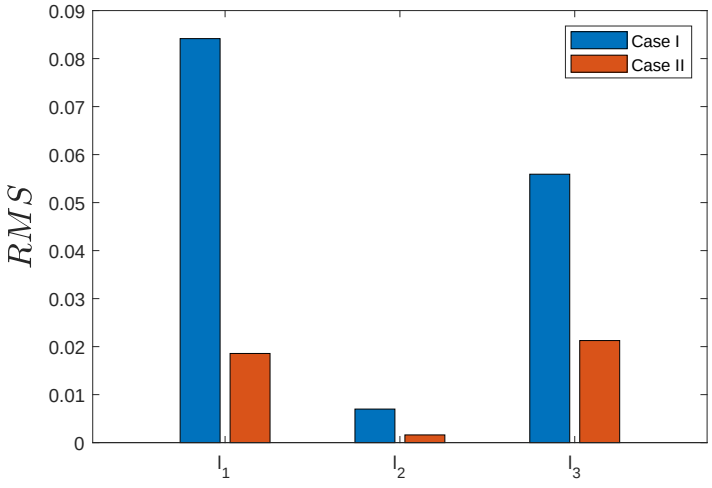

Fig. 15: RMS of the cable length error

base forward and backward and (II) moving the crane up and down. Kinetostatic models of both schemes were derived, and the robot's workspace was plotted by considering the ZMP. A trajectory traced by the end-effector was generated by using the fifth-degree polynomial. Following this trajectory, the next positions of cable exit points were always changed, represented by the continuous change of the mobile base position and the crane length of the reconfiguration schemes I and II, respectively. An optimization was employed to define the set of mobile base positions and the crane length such that the whole system was always in equilibrium. A prototype of the CDPR using three mobile cranes was fabricated. An experiment was performed on the developed prototype, and it confirmed that both reconfiguration schemes were able to prevent the robot from tipping over when executing a given task. The results also revealed that the cable tensions and the error of cable lengths of reconfiguration II are lower than those of reconfiguration I, which shows that reconfiguration II is potentially more applicable.

References

1. Andreas Pott, Hendrick Mütherich, Werner Kraus, Valentine Schmidt, Philipp Miermeister, and Alexander Verl. Ipanema: a family of cable-driven parallel robots for industrial applications. *Cable-Driven Parallel Robots*, pages 119–134, 2013.
2. Johann Lamaury, Marc Gouttefarde, Ahmed Chemori, and Pierre-Elie Hervé. Dual-space adaptive control of redundantly actuated cable-driven parallel robots. In *2013 IEEE/RSJ International Conference on Intelligent Robots and Systems*, pages 4879–4886. IEEE, 2013.
3. Philipp Tempel, Pierre-Elie Herve, Olivier Tempier, Marc Gouttefarde, and Andreas Pott. Estimating inertial parameters of suspended cable-driven parallel robots—use case on cogiro. In *2017 IEEE International Conference on Robotics and Automation (ICRA)*, pages 6093–6098. IEEE, 2017.
4. Franklin Okoli, Yuchuan Lang, Olivier Kermorgant, and Stéphane Caro. Cable-driven parallel robot simulation using gazebo and ros. In *ROMANSY 22–Robot Design, Dynamics and Control: Proceedings of the 22nd CISM IFToMM Symposium, June 25-28, 2018, Rennes, France*, pages 288–295. Springer, 2019.
5. Saeed Abdolshah, Damiano Zanotto, Giulio Rosati, and Sunil K Agrawal. Optimizing stiffness and dexterity of planar adaptive cable-driven parallel robots. *Journal of Mechanisms and Robotics*, 9(3):031004, 2017.
6. Houssein Lamine, Lotfi Romdhane, Houssem Saafi, and Sami Bennour. Design-to-workspace synthesis of a cable robot used in legs training machine. *Robotica*, 38(9):1703–1714, 2020.
7. Andreas Pott. *Cable-Driven Parallel Robots*. Springer Cham, 2018.
8. Marc Gouttefarde, Jean-Pierre Merlet, and David Daney. Wrench-feasible workspace of parallel cable-driven mechanisms. In *Proceedings 2007 IEEE International Conference on Robotics and Automation*, pages 1492–1497. IEEE, 2007.
9. Hussein Hussein, João Cavalcanti Santos, Jean-Baptiste Izard, and Marc Gouttefarde. Smallest maximum cable tension determination for cable-driven parallel robots. *IEEE Transactions on Robotics*, 37(4):1186–1205, 2021.
10. Tahir Rasheed, Philip Long, David Marquez-Gamez, and Stéphane Caro. Available wrench set for planar mobile cable-driven parallel robots. In *2018 IEEE International Conference on Robotics and Automation (ICRA)*, pages 962–967. IEEE, 2018.
11. Tahir Rasheed, Philip Long, and Stéphane Caro. Wrench-feasible workspace of mobile cable-driven parallel robots. *Journal of Mechanisms and Robotics*, 12(3), 2020.
12. Richard Verhoeven. *Analysis of the workspace of tendon-based Stewart platforms*. PhD thesis, Duisburg, Essen, Univ., Diss., 2004, 2004.
13. Clément Gosselin. Global planning of dynamically feasible trajectories for three-dof spatial cable-suspended parallel robots. *Cable-Driven Parallel Robots*, pages 3–22, 2013.
14. Yi Fang, Jie Hu, Wenhai Liu, Quanquan Shao, Jin Qi, and Yinghong Peng. Smooth and time-optimal s-curve trajectory planning for automated robots and machines. *Mechanism and Machine Theory*, 137:127–153, 2019.
15. Priyam A Parikh, Reena Trivedi, and Jatin Dave. Trajectory planning for the five degree of freedom feeding robot using septic and nonic functions. *International Journal of Mechanical Engineering and Robotics Research*, 9(7):1043–1050, 2020.
16. Tai Duc Nguyen, Phuc Thanh Phan, and Thinh Truong Nguyen. Design dynamic models for cable robot spraying pesticides in agricultural production. *International Journal of Mechanical Engineering and Robotics Research*, 9(4):516–520, 2020.
17. Ruobing Wang and Yangmin Li. Analysis and multi-objective optimal design of a planar differentially driven cable parallel robot. *Robotica*, 39(12):2193–2209, 2021.
18. Lorenzo Gagliardini, Stéphane Caro, Marc Gouttefarde, and Alexis Girin. Discrete reconfiguration planning for cable-driven parallel robots. *Mechanism and Machine Theory*, 100:313–337, 2016.
19. Giulio Rosati, Damiano Zanotto, and Sunil K Agrawal. On the design of adaptive cable-driven systems. 2011.
20. Satoshi Tadokoro, Richard Verhoeven, Manfred Hiller, and Toshi Takamori. A portable parallel manipulator for search and rescue at large-scale urban earthquakes and an identification algorithm for the installation in unstructured environments. *Proceedings 1999 IEEE/RSJ International Conference on Intelligent Robots and Systems (IROS)*, 2:1222–1227, 1999.

21. Damiano Zanotto, Giulio Rosati, Simone Minto, and Aldo Rossi. Sophia-3: A semi adaptive cable-driven rehabilitation device with a tilting working plane. *IEEE Transactions on Robotics*, 30(4):974–979, 2014.
22. Dinh Quan Nguyen and Marc Gouttefarde. Study of reconfigurable suspended cable-driven parallel robots for airplane maintenance. In *2014 IEEE/RSJ International Conference on Intelligent Robots and Systems*, pages 1682–1689. IEEE, 2014.
23. Paul Bosscher, Robert L Williams II, L Sebastian Bryson, and Daniel Castro-Lacouture. Cable-suspended robotic contour crafting system. *Automation in construction*, 17(1):45–55, 2007.
24. Ilija Vukorep. Autonomous big-scale additive manufacturing using cable-driven robots. In *ISARC. Proceedings of the International Symposium on Automation and Robotics in Construction*, volume 34. IAARC Publications, 2017.
25. Tobias Bruckmann, Christopher Reichert, Michael Meik, Patrik Lemmen, Arnim Spengler, Hannah Mattern, and Markus König. Concept studies of automated construction using cable-driven parallel robots. In *Cable-Driven Parallel Robots: Proceedings of the Third International Conference on Cable-Driven Parallel Robots*, pages 364–375. Springer, 2018.
26. Roland Boumann, Patrik Lemmen, Robin Heidel, and Tobias Bruckmann. Optimization of trajectories for cable robots on automated construction sites. In *ISARC. Proceedings of the International Symposium on Automation and Robotics in Construction*, volume 37, pages 465–472. IAARC Publications, 2020.
27. Tahir Rasheed, Philip Long, Adolfo Suarez Roos, and Stéphane Caro. Optimization based trajectory planning of mobile cable-driven parallel robots. In *2019 IEEE/RSJ International Conference on Intelligent Robots and Systems (IROS)*, pages 6788–6793. IEEE, 2019.
28. Bin Zi, Jun Lin, and Sen Qian. Localization, obstacle avoidance planning and control of a cooperative cable parallel robot for multiple mobile cranes. *Robotics and Computer-Integrated Manufacturing*, 34:105–123, 2015.
29. Nicolò Pedemonte, Tahir Rasheed, David Marquez-Gamez, Philip Long, Étienne Hocquard, Francois Babin, Charlotte Fouché, Guy Caverot, Alexis Girin, and Stéphane Caro. Fastkit: A mobile cable-driven parallel robot for logistics. *Advances in Robotics Research: From Lab to Market: ECHORD++: Robotic Science Supporting Innovation*, pages 141–163, 2020.
30. Tahir Rasheed, Philip Long, David Marquez-Gamez, and Stéphane Caro. Kinematic modeling and twist feasibility of mobile cable-driven parallel robots. In *Advances in Robot Kinematics 2018 16*, pages 410–418. Springer, 2019.
31. Cyril Alias, Ilia Nikolaev, Eduardo Garduño Correa Magallanes, and Bernd Noche. An overview of warehousing applications based on cable robot technology in logistics. In *2018 IEEE International Conference on Service Operations and Logistics, and Informatics (SOLI)*, pages 232–239. IEEE, 2018.
32. Tahir Rasheed, Philip Long, David Marquez-Gamez, and Stéphane Caro. Tension distribution algorithm for planar mobile cable-driven parallel robots. In *Cable-Driven Parallel Robots: Proceedings of the Third International Conference on Cable-Driven Parallel Robots*, pages 268–279. Springer, 2018.
33. Shuhai Jiang, Wei Song, Zhongkai Zhou, and Shangjie Sun. Stability analysis of the food delivery robot with suspension damping structure. *Heliyon*, 8(12), 2022.
34. Pegnwen Xiong, Aiguo Song, Peng Ji, and Xinjing Huang. Study on ability of a mobile tracked robot for stair-climbing based on static analysis. In *2015 IEEE International Conference on Cyber Technology in Automation, Control, and Intelligent Systems (CYBER)*, pages 1327–1332. IEEE, 2015.
35. Chunyang Zhang, Xianzhi Jiang, Minliang Teng, and Jun Teng. Research on gait planning and static stability of hexapod walking robot. In *2015 8th International Symposium on Computational Intelligence and Design (ISCID)*, volume 2, pages 176–179. IEEE, 2015.
36. Xueshan Gao, Dengqi Cui, Wenzeng Guo, Yu Mu, and Bin Li. Dynamics and stability analysis on stairs climbing of wheel–track mobile robot. *International Journal of Advanced Robotic Systems*, 14(4):1729881417720783, 2017.
37. Tae Hyeong Lim, Yong Seok Kim, Jong Hwan, Hong Sun Lee, and Soon Yong Yang. Development of tipping-over rate computation system for hydraulic excavator having crane function. In *Proceedings. The 8th Russian-Korean International Symposium on Science and Technology, 2004. KORUS 2004.*, volume 3, pages 76–79. IEEE, 2004.
38. Yan Jia, Xiao Luo, Baoling Han, Guanhao Liang, Jiaheng Zhao, and Yuting Zhao. Stability criterion for dynamic gaits of quadruped robot. *Applied Sciences*, 8(12):2381, 2018.
39. Philippe Sardain and Guy Bessonnet. Forces acting on a biped robot. center of pressure-zero moment point. *IEEE Transactions on Systems, Man, and Cybernetics-Part A: Systems and Humans*, 34(5):630–637, 2004.
40. Jason Pusey, Abbas Fattah, Sunil Agrawal, and Elena Messina. Design and workspace analysis of a 6–6 cable-suspended parallel robot. *Mechanism and machine theory*, 39(7):761–778, 2004.